nature chemistry

Article

https://doi.org/10.1038/s41557-023-01315-w

Aromatic pentaamide macrocycles bind anions with high affinity for transport across biomembranes

Received: 15 January 2022

Accepted: 8 August 2023

Published online: 09 October 2023



Ruikai Cao^{1,6}, Robert B. Rossdeutcher^{1,6}, Yulong Zhong ^{1,6}, Yi Shen ², Daniel P. Miller ³, Thomas A. Sobiech¹, Xiangxiang Wu ⁴, Laura Sánchez Buitrago ³, Karishma Ramcharan ³, Mark I. Gutay⁵, Miriam Frankenthal Figueira ⁵, Pia Luthra ³, Eva Zurek ¹, Thomas Szyperski¹, Brian Button⁵, Zhifeng Shao ² & Bing Gong ¹

The convergent positioning of functional groups in biomacromolecules leads to good binding, catalytic and transport capabilities. Synthetic frameworks capable of convergently locking functional groups with minimized conformational uncertainty—leading to similar properties—are highly desirable but rare. Here we report C5-symmetric aromatic pentaamide macrocycles synthesized in one pot from the corresponding monomers. Their crystal structures reveal a star-shaped, fully constrained backbone that causes ten alternating NH/CH hydrogen-bond donors and five large amide dipoles to orient towards the centre of the macrocycle. With a highly electropositive cavity in a high-energy unbound state, the macrocycles bind anions in a 1:1 stoichiometry in solution, with high affinity for halides and very high affinity for oxoanions. We demonstrate that such macrocycles are able to transport anions across lipid bilayers with a high chloride selectivity and restore the depleted airway surface liquid of cystic fibrosis airway cell cultures.

Molecular and supramolecular structures with multiple functional groups convergently placed at defined positions occur ubiquitously in nature. Amassing multiple non-covalent forces¹, such structures exhibit sophisticated functions from ligand binding and mass transport to signal transduction that are still beyond the reach of synthetic constructs. The potassium channel KcsA² and the water channel aquaporin 1 (ref. 3) achieve excellent efficiency and selectivity in transporting potassium ions and water molecules, respectively, with a selectivity filter defined by converged polar groups and dipoles. The selectivity filter of anion Cl⁻ channel ClC is defined by converged NH, CH and OH groups towards the bound chloride⁴. The convergent functional groups

are also utilized by ligand-binding proteins such as the sulfate-binding protein of S. $typhimurium^5$ that binds the sulfate ion, an anion with a large hydration enthalpy (-258 kcal mol $^{-1}$), in high affinity (association constant $K_a = 8.3 \times 10^6$ M $^{-1}$ at pH 8.3) in water. By forming seven neutral hydrogen bonds with the sulfate ion, involving five main chain peptide NH groups, a serine OH and the indole NH of a tryptophan, the sulfate-binding protein demonstrates that properly placed neutral hydrogen bonds can result in extraordinary anion binding affinities.

Anions have attracted wide interest in molecular recognition because of their importance in biology, medicine and the environment⁶. In contrast to cations, anions, with a variety of sizes and shapes,

Department of Chemistry, University at Buffalo, The State University of New York, Buffalo, NY, USA. 2State Key Laboratory of Systems Medicine for Cancer, School of Biomedical Engineering, Shanghai Jiao Tong University, Shanghai, China. Department of Chemistry, Hofstra University, Hempstead, NY, USA. Academy of Chinese Medical Science, Henan University of Chinese Medicine, Zhengzhou, Henan, China. Marsico Lung Institute, University of North Carolina School of Medicine, Chapel Hill, NC, USA. These authors contributed equally: Ruikai Cao, Robert B. Rossdeutcher, Yulong Zhong. Se-mail: zfshao@sjtu.edu.cn; bgong@buffalo.edu

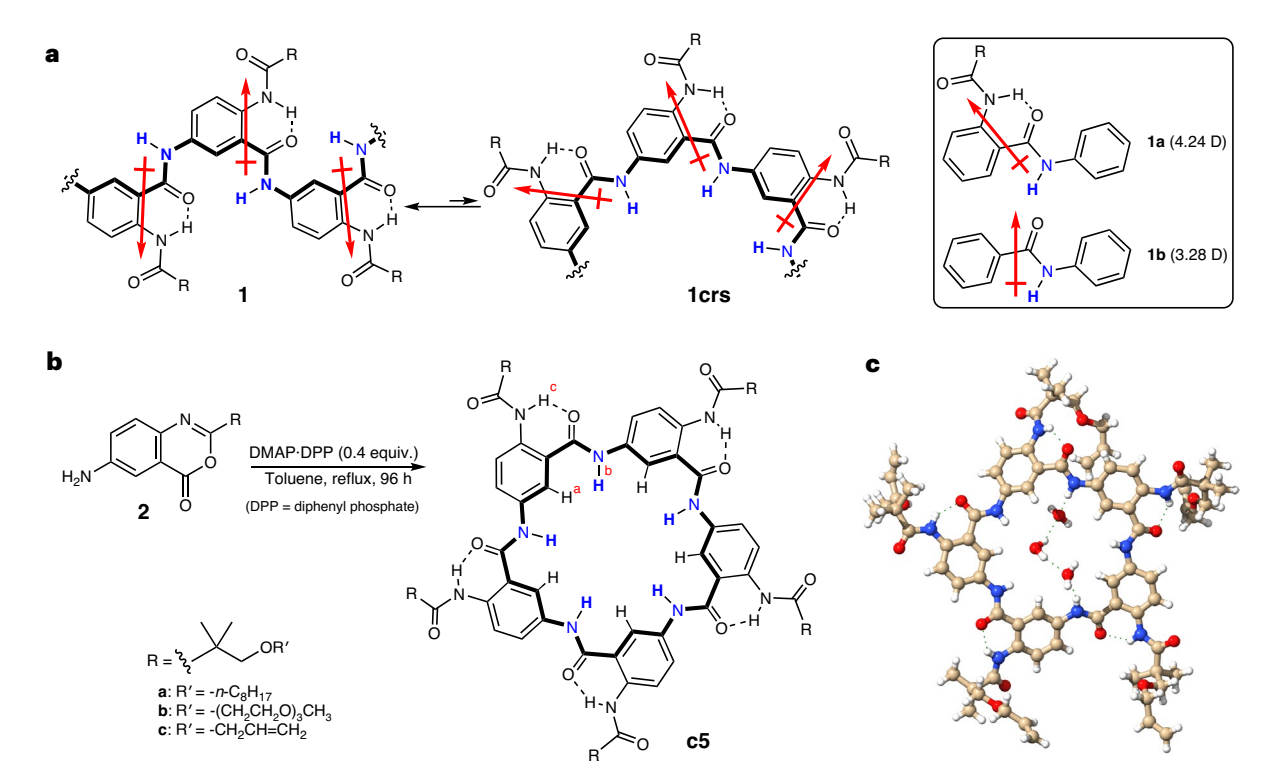


Fig. 1 | Linear oligoamide 1 and macrocycles c5 consisting of basic residues derived from 5-amino-N-acylanthranilic acid. a, Linear oligoamides 1 with the energetically unfavourable crescent conformation 1crs and the overall electrical dipole moments of amides 1a and 1b in the predicted conformations from DFT calculations performed with the ADF 57 software package. b, Synthesis of

macrocycles ${\bf c5a-c}$ based on a one-pot macrocyclization process. In ${\bf a}$ and ${\bf b}$, the backbones of the linear and cyclic oligoamides are highlighted with thick bonds and N–H groups are highlighted in blue. ${\bf c}$. Crystal structure of ${\bf c5c}$ in which two of the five side chains are disordered with water molecules being hydrogen bonded to the backbone NH groups.

have been largely elusive for synthetic receptors until recent years. Anion recognition requires the convergent alignment of binding groups, especially hydrogen-bond donors 4,5 . Typical anion receptors include linear or branched molecules carrying hydrogen-bond donors. They are based on the NH groups of amides, ureas, pyrroles, amines and ammoniums 7 and, more recently, have included halogen bonds 8,9 with which the entropic costs for hydrogen-bond donors to converge on anions have to be compensated by the enthalpic gains from non-covalent interactions. A promising structures including multiple functional groups is based on rigid structures including molecular clefts 10 , foldamers 11,12 and macrocycles $^{13-15}$ with unique and often remarkable capabilities of selectively and tightly binding guest species.

Shape-persistent macrocycles are especially powerful in converging functional groups with non-deformable cavities of defined sizes. Flood and co-workers demonstrated the formation of stable 2:1 sandwich complexes of large anions with a rigid macrocycle having convergent aromatic CH groups¹⁶ and the 1:1 binding of the chloride ion with another macrocycle with convergent triazole and phenyl CH groups¹⁷. These systems, along with those reported by Anslyn and co-workers¹⁸, Sessler and Davies¹⁹ and Gale and co-workers²⁰, demonstrate that rigid cyclic hosts with convergent hydrogen-bond donors, even those involving aromatic CH groups that are regarded as 'weak' donors²¹, could achieve strong binding for anions.

Among hydrogen-bond donors, the amide NH functionality is much preferred in the design of anion receptors for its exceptional hydrogen-bonding capability and synthetic accessibility^{22–24}. With rigid residues linked by amide linkages, aromatic oligoamide macrocycles can organize multiple binding elements to achieve strong anion binding. Ideally, the macrocyclic backbones should be rigid and fully constrained, with restricted rotation around each backbone aryl–amide single bond, so that the ambiguity in local orientation associated with

the amide groups could be minimized or even eliminated. However, due to the structural limitations of the amide group, most known amide-based anion receptors have significant conformational flexibility, along with unhindered rotation around the aryl–amide single bonds, leading to compromised binding affinity and selectivity. Moreover, incorporating amide NH units into anion receptors inevitably brings along amide C=O groups engaging in undesired hydrogen-bonding interactions that result in self-aggregation and poor solubility.

Choi and Hamilton reported their seminal work on a rigid aromatic triamide macrocycle with an ~5 Å cavity that binds dihydrogen phosphate $(K_a \approx 10^4 \,\mathrm{M}^{-1})$ in deuterated dimethyl sulfoxide (DMSO)- d_6)²⁵ without rotational restriction of the backbone aryl-amide single bonds. While we have succeeded in constructing aromatic oligoamide macrocycles with rigidly placed, convergent backbone amide C=O groups²⁶, the inherent limitation of the amide group precluded the creation of aromatic oligoamide macrocycles capable of convergently locking NH groups. In fact, the design of rigid hosts with preorganized, convergently placed amide NH groups for anion binding remains a daunting conceptual and synthetic challenge. To address this challenge, we have now successfully designed and synthesized the star-shaped macrocycles c5 featuring a constrained backbone that locks multiple amide NH and CH groups into an unambiguous, convergent placement. Macrocycles c5 represent the newest member of a family of cyclic compounds including MacLachlan and co-worker's camperstarenes¹⁴, Zeng and co-worker's pentamers¹⁵ and Flood and co-worker's cyanostars¹⁶ with a rare C_5 symmetry. The non-deformable cavity of **c5** defined by these NH and CH donors with inwardly pointing amide dipoles is highly electropositive and predisposed for anion accommodation. The resultant anion binders could find important applications such as serving as remedies for malfunctioning anion transport found in a variety of diseases⁶.

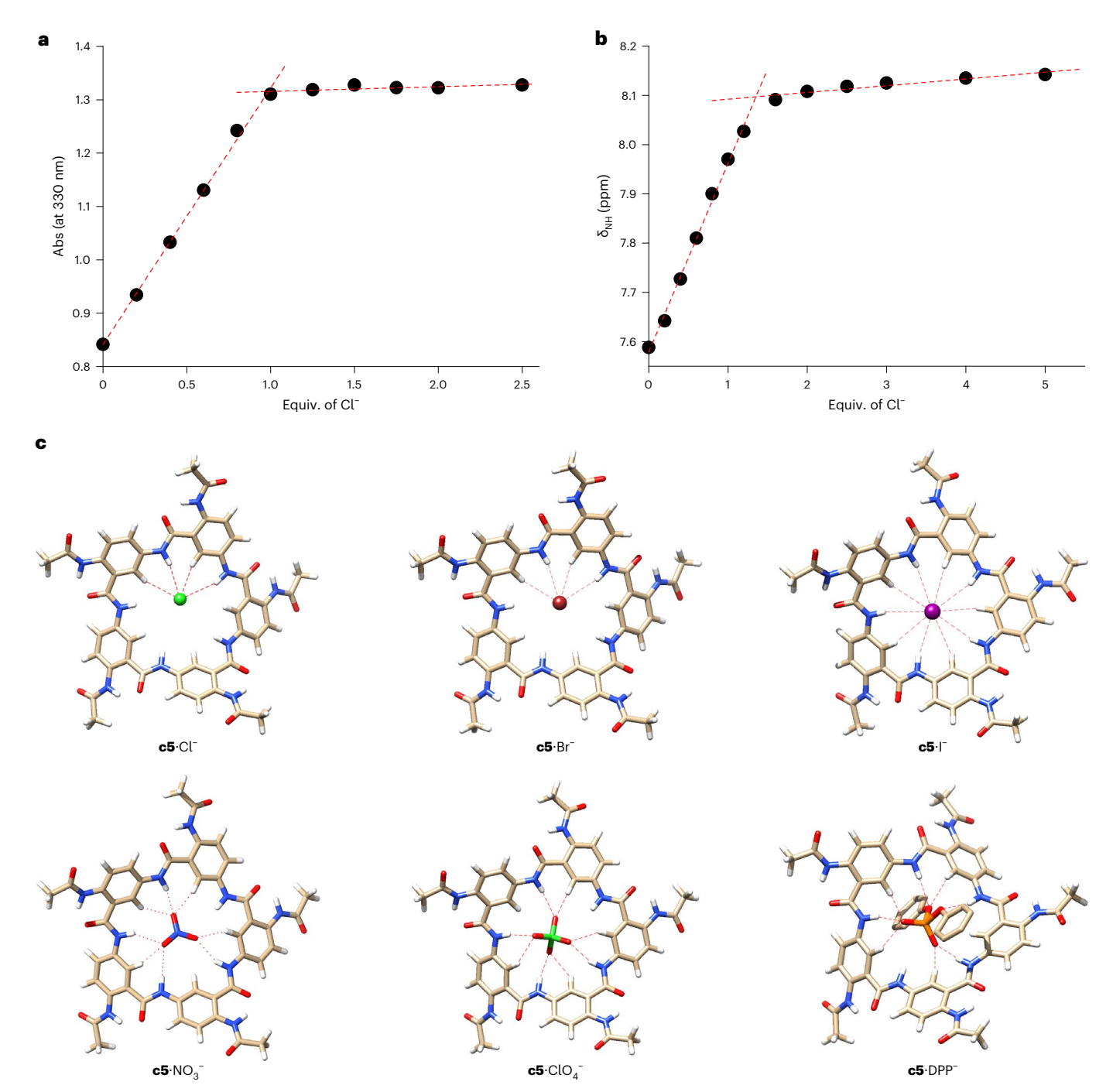


Fig. 2 | Binding stoichiometry of macrocycles c5 with anions. a, Changes in the 330 nm absorbance of c5a (20 μ M) titrated with 0–2.5 equiv. of TBA*Cl⁻ in CH₃OH:CHCl₃ (5:95, v/v). b, Changes in the chemical shifts of endocyclic protons a of c5a titrated with 0–5 equiv. of TBA*Cl⁻ in DMSO-d₀:CDCl₃ (1:99, v/v). In a and b, the abrupt change in absorbance or chemical shift indicates that the

stoichiometry of the binding is 1:1. **c**, Optimized structures of the 1:1 complexes of **c5** with Cl¯, Br¯, l¯, NO $_3$ ¯, ClO $_4$ ¯ and DPP¯. In each complex, the CH/NH protons and the anion that are within van der Waals contact distances ($d_{\text{H--O}} \le 2.8 \text{ Å}$; $d_{\text{H--Cl}} \le 3.0 \text{ Å}$; $d_{\text{H--Br}} \le 3.1 \text{ Å}$; $d_{\text{H--I}} \le 3.3 \text{ Å}$) are indicated by red dashed lines. The structures were computationally optimized in vacuum⁵⁷.

Results and discussion

Design and synthesis of cyclic aromatic pentaamides c5

We recently reported anion-binding aromatic oligoamide foldamers sharing general structure **1** (Fig. **1a**)²⁷. The intramolecular hydrogen bonds in **1** serve to (1) partially rigidify the oligoamide backbone, (2) prevent the backbone amide C=O groups from engaging in additional hydrogen-bonding interaction and (3) free the backbone amide NH groups to form hydrogen bonds with guest species. As shown in Fig. **1a**, amide **1a**, the basic unit of **1**, has a large dipole moment (4.24 D) contributed by the two hydrogen-bonded amide groups, while

amide **1b** has a smaller dipole moment (3.28 D) as it lacks a sidechain amide group. Thus, oligoamide **1** adopts a conformation with the adjacent amide dipoles aligned in an energetically favourable antiparallel orientation. Like other anion-binding foldamers ^{8,28-32}, upon binding an anion, oligoamide **1** folds into conformation **1crs** in which the backbone NH groups, along with the positive ends of the amide dipoles, are oriented to define an electropositive cavity²⁷. The entropic barrier for **1** to adopt conformation **1crs** leads to modest anion-binding affinities that increase with the number of NH groups²⁷.

Table 1	Association constants K	ζ (M ⁻¹) for the 1:1 com	plexes of c5a with	various anions at 25°C
---------	-------------------------	--------------------	-------------------	--------------------	------------------------

	D: . /å\		71100 01101 (7 07 1)hs	OD ON ODOL (00 00 /)	all all all (Table 1) ha
	Diameter (Å)	DMSO-d ₆ :CDCl ₃ (15:85, v/v) ^a	DMSO:CHCl ₃ (5:95, v/v) ^{b,c}	CD ₃ CN:CDCl ₃ (80:20, v/v) ^a	CH ₃ CN:CHCl ₃ (5:95, v/v) ^{b,c}
Cl-	3.36	$(4.31\pm0.12)\times10^3$	$(1.60 \pm 0.10) \times 10^4$	$(8.25\pm0.59)\times10^{4}$	$(2.34\pm0.24)\times10^6$
Br ⁻	3.80	(9.82±1.08) × 10 ³	(1.37±0.04) × 10 ⁴	(4.98±0.30)×10 ⁴	(1.79±0.34)×10 ⁷
NO ₃ -	4.00	(1.57±0.13) × 10 ⁵	$(1.30\pm0.10)\times10^6$	>10 ⁶	$(1.38 \pm 0.21) \times 10^{9d}$
BF ₄	4.10	(4.73±0.38)×10 ⁴	(8.70±0.40)×10 ⁵	(2.10±0.23)×10 ^{5f}	(3.09±0.45)×10 ^{8d}
Γ	4.22	(2.73±0.17) × 10 ⁴ (3.77±0.25) × 10 ^{4b} (1.18±0.03) × 10 ^{4c}	(1.83±0.08)×10 ⁵	(5.96±0.89)×10 ^{5f}	$(7.78\pm4.26)\times10^{7}$ $(6.67\pm0.81)\times10^{7e}$
ClO ₄	4.50	(5.74±0.51) × 10 ⁴ (9.60±0.76) × 10 ^{4b} (1.90±0.02) × 10 ^{4c}	(4.50±0.50) ×10 ⁵	(4.27±0.67)×10 ^{5f}	(4.96±0.76)×10 ^{8d}
IO ₄	4.62	(1.18±0.08) × 10 ⁴	(1.72±0.05) × 10 ⁵	(4.24±0.21) × 10 ⁴	(2.54±0.22)×10 ⁷
PF ₆	4.84	Not detected	(2.80±0.20)×10 ⁴	(3.70±0.22)×10 ³	(1.23±0.17)×10 ⁷

Measured at 298 K. Determined by NMR titrations by fitting the chemical shift changes of both protons a and b unless indicated otherwise. Determined by triplicate NMR titrations. Determined by ITC measurements. Determined by two-step competition ITC experiments with PF₆ as the competitor. Determined by two-step competition ITC experiments with Cl as the competitor. Value based on chemical shift changes of CH protons a only due to large errors involving NH protons b.

Cyclizing oligoamide 1 can yield macrocycles with 5 or 6 residues due to the ~120° bond angles defined by the sp^2 -hybridized C and N atoms. Density functional theory (DFT) calculations of the five-residue macrocycle c5 (Fig. 1b) reveal a slightly puckered conformation (Supplementary Fig. 1a) but the six-residue macrocycle has a significantly crinkled shape, indicating a strained structure (Supplementary Fig. 1b). The hindered rotation of the aryl-amide single bonds in the cyclic backbone of c5 greatly reduces the conformational flexibility of the backbone. The intramolecular hydrogen bonds along the backbone also prevent the amide groups from flipping 180°, forcing the amide NH and phenyl CH groups to point to the interior of the macrocycle (Fig. 1b,c and Supplementary Fig. 1a). With its highly electropositive cavity, as shown with DFT computed Hirshfeld charges of +0.12 e and +0.04 e for each of the NH and CH protons, macrocycle c5 is in a high-energy unbound state³¹ in comparison to its acyclic counterpart (Supplementary Fig. 2). This is due to the repulsion between amide dipoles and between the partially charged endocyclic NH and CH protons brought into close proximity by the cyclized backbone. As a result, macrocycle **c5** is predisposed for anion binding.

Macrocycle **c5a** was first synthesized in an overall yield of ~24% by cyclizing a linear oligoamide precursor prepared based on an amide-coupling method we recently developed (Supplementary Scheme 1)²⁷. Subsequently, we were able to develop a much more efficient one-pot synthesis of **c5a** (~45% yield) involving heating **2a** (2 mM) and a 1:1 mixture of diphenyl phosphate (DPP) and 4-dimethylaminopyridine (DMAP) (40 mol%) in toluene under reflux (Fig. 1b and Supplementary Scheme 2; see Methods section 'One-pot synthesis of macrocycles **c5**' for details). This one-pot procedure, which was also effective in the production of **c5b** and **c5c**, provides a simple and scalable route allowing structural tuning and optimization for preparing **c5** derivatives carrying different sidechains.

Crystal structures and solution properties of c5

Compound **c5a** was crystallized from DMSO by slow cooling and **c5c** was obtained from CHCl₃:CH₃CN (1:1, v/v) by slow evaporation of the solvent. The crystal structures of **c5a** (Supplementary Fig. 3) and **c5c** (Fig. 1c) have overall planar conformations resembling the energy-minimized structure of **c5** (Supplementary Fig. 1a). Similar to the CH and NH groups constituting the selectivity filter of ClC Cl-channels⁴, all of the endocyclic NH and CH groups of **c5c** are oriented towards the centre of the macrocycle (Fig. 1c), defining a cavity of -6.8 Å (H to H) or -4.6 Å (van der Waals). The backbone amide groups and their flanking benzene rings have dihedral angles of 0 to 40°, leading to a slightly puckered conformation that presumably alleviates the

repulsion between the amide dipoles and between the partially positive endocyclic hydrogens. The intramolecular hydrogen bonds also enforce the coplanar alignment of the sidechain amide groups and the benzene rings. In the cavity, three water molecules are hydrogen bonded to amide protons b. The crystal structure of **c5a** (Supplementary Fig. 3) shows similar features, with all of its endocyclic CH and NH groups being convergently placed. The backbone of **c5a** is more puckered than that of **c5c**, probably owing to different crystal packing caused by the sidechains. In the cavity of **c5a**, two DMSO molecules are hydrogen bonded to two NH groups. Examining the packing of **c5c** indicates that adjacent macrocycles have about one residue of their backbones being stacked at ~3.4 Å (Supplementary Fig. 4). Such a small contact surface between two adjacent macrocycles is likely to be caused by the repulsive interactions between the amide dipoles, should the macrocycles stack face-to-face.

The lack of strong stacking between the macrocycles is reflected by the overall good solubility of macrocycles **c5a,b** in many solvents including chloroform. This contrasts with the poor solubilities typical of most acyclic and cyclic aromatic oligoamides. With the polar sidechains having tri(ethylene glycol) tails, **c5b** also has a reasonable solubility (-1 mM) in water.

High-affinity anion recognition by macrocycles c5

With their backbone NH and CH groups being highly preorganized, macrocycles $\mathbf{c5}$ should bind anions of different properties. Eleven anions including halides Cl $^-$, Br $^-$ and I $^-$, the weakly coordinating BF $_4$ $^-$ and PF $_6$ $^-$, oxoanions NO $_3$ $^-$, ClO $_4$ $^-$, IO $_4$ $^-$, HSO $_4$ $^-$, methyl phenylphosphonate (MPP $^-$) and diphenyl phosphate (DPP $^-$), with a variety of sizes, shapes, charge densities and hydrogen-bonding capabilities, were examined for their interaction with $\mathbf{c5}$.

The anion binding stoichiometry of macrocycles **c5a** and **c5c** was analysed with ultraviolet–visible (UV–vis) and 1 H NMR titrations in different solvents and with high-resolution mass spectra (HRMS) recorded in negative ion mode. Titrating **c5a** with the tetrabutylammonium (TBA $^+$) salt of chloride (Fig. 2a) or other anions (Supplementary Fig. 5) revealed a linear dependence of the UV–vis absorbance of **c5a** that exhibits an abrupt change around 330 nm at 1 equiv. of each anion, indicating a 1:1 binding ratio.

In CDCl₃ containing 5% DMSO-d₆, the chemical shifts of phenyl CH protons a of **c5a** upon titrating with 0–5 equiv. of TBA⁺Cl⁻ exhibited the same abrupt change around 1 equiv. of TBA⁺Cl⁻ (Fig. 2b and Supplementary Fig. 6a) or TBA⁺Br⁻ (Supplementary Fig. 6b), confirming the 1:1 binding stoichiometry. Consistent with 1:1 binding, titrating **c5a** with Γ or ClO_4^- in the same solvent gave two separate sets of Γ 1 NMR

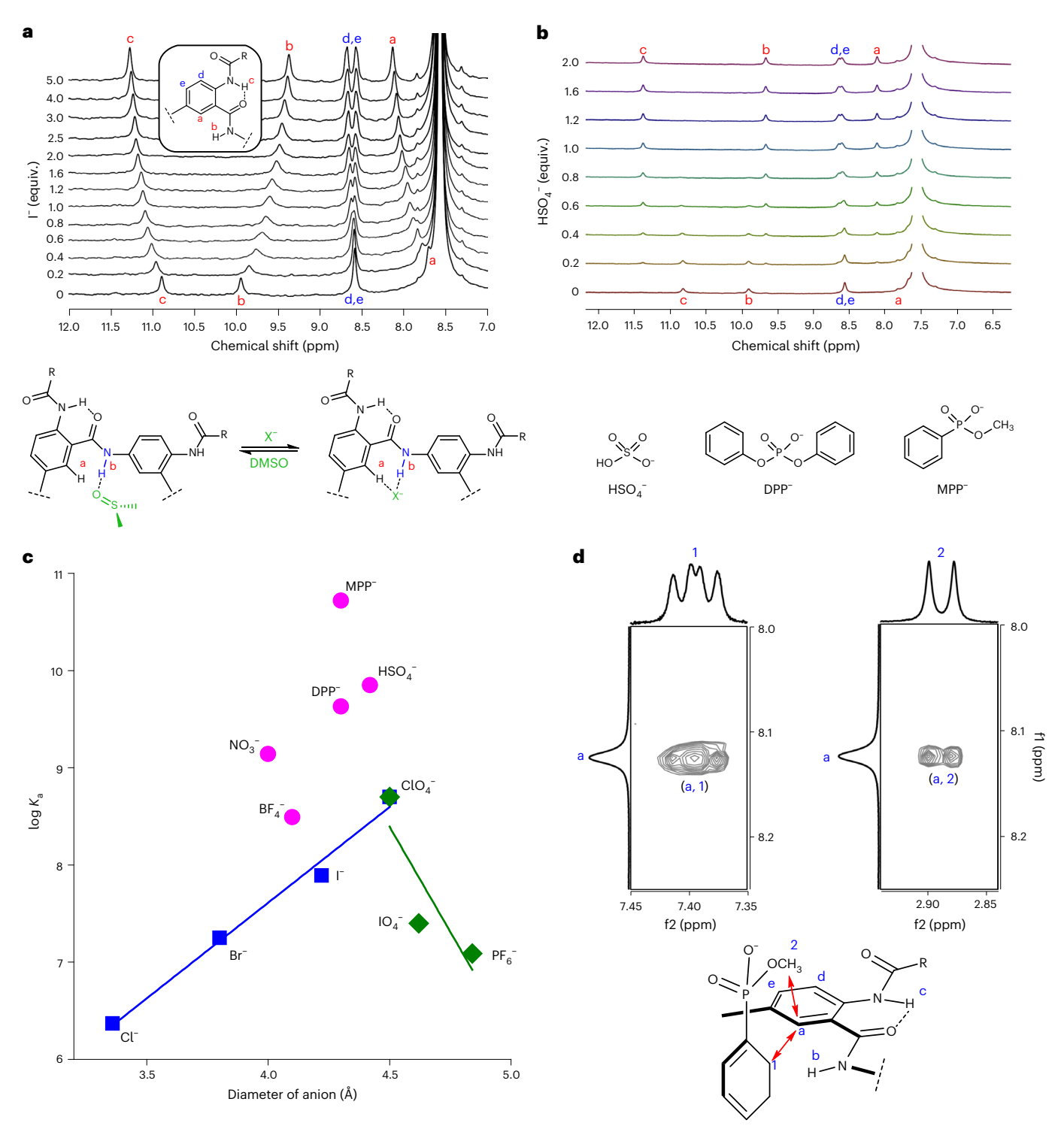


Fig. 3| ¹**H NMR spectra and association constants** ($\log K_a$) of c5a. a, Top: ¹H NMR spectra of c5a (0.1 mM) titrated with 0 to 5 equiv. of TBA*T in DMSO-d₆:CDCl₃ (15:85, v/v). Amide protons b and c, along with aromatic protons a, which exhibit significant shifts with different ratios of I⁻, are labelled in red. Aromatic protons d and e, which experience only small shifts with changing ratios of I⁻, are labelled in blue. Bottom: the solvated cavity of c5 with DMSO molecule(s) hydrogen bonded to amide protons b (left) and the desolvated cavity of c5 occupied by an anion (X') that forms hydrogen bonds with amide protons b and phenyl protons a (right). The different shifts of protons a and b suggest that amide protons a are involved in hydrogen bonding with DMSO molecules. b, Top: ¹H NMR spectra of c5a

 $(0.1\,\text{mM})$ titrated with 0 to 2 equiv. of TBA*HSO₄- in DMSO-d₆:CDCl₃ (15:85, v/v), indicating that the free and bound forms of **c5a** are in close exchange. Bottom: structures of three oxoanions. **c**, Association constants (log K_a) of **c5a** with the anions in CH₃CN:CHCl₃ (5:95) reveal that the affinities of **c5a** for halides along with ClO₄-, IO₄- and PF₆- follow a size-dependent trend while the affinities for BF₄- and four other oxoanions do not follow any size-dependent trend. **d**, Partial 2D (ROESY) spectra of the 1:1 mixture of **c5a** and TBA·MPP in DMSO-d₆ (20 mM, 500 MHz, mixing time = 0.4 s, 25 °C) demonstrate the binding of MPP- inside the cavity of **c5a**.

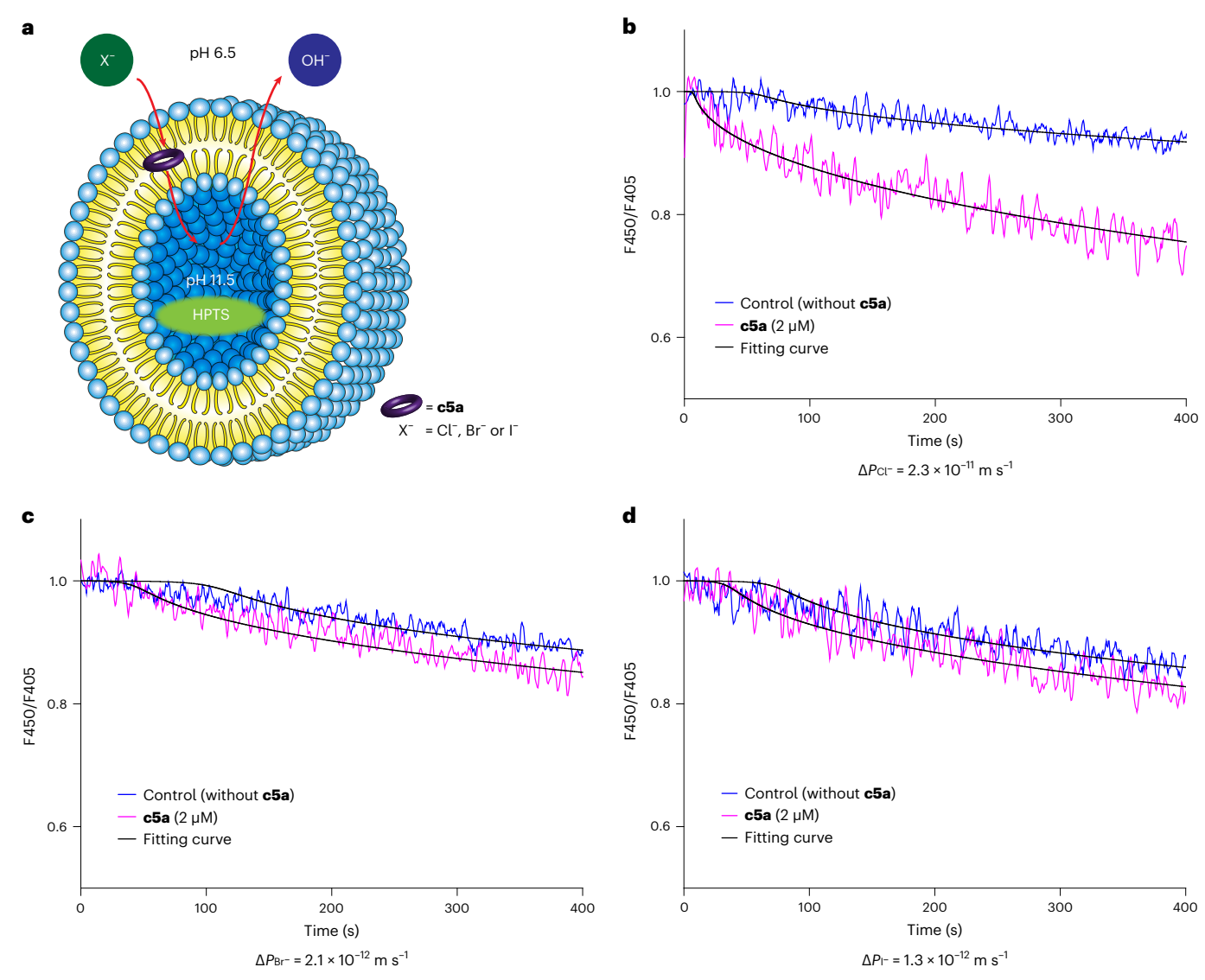


Fig. 4 | **Transmembrane transport of halide ions promoted by macrocycle c5a. a**, Dissipation of the pH gradient quenches the emission of the pH-sensitive dye HPTS entrapped in 1-palmitoyl-2-oleoyl-sn-glycero-3-phosphocholine (POPC) LUVs. \mathbf{b} - \mathbf{d} , Normalized ratio of time-lapse fluorescence emission intensities of $\mathsf{Cl}^-(\mathbf{b})$, $\mathsf{Br}^-(\mathbf{c})$ and $\mathsf{I}^-(\mathbf{d})$ transport facilitated by $\mathbf{c5a}$, along with the control curves (in blue) measured with vesicles in the absence of $\mathbf{c5a}$. A larger difference between the transport facilitated by $\mathbf{c5a}$ versus control means more enhancement occurred by $\mathbf{c5a}$ and a conclusion that $\mathbf{c5a}$ enhances the transmembrane transport of Cl^- the most and I^- the least could be obtained.

The transport of halides was examined by measuring the fluorescence excitation/emission wavelengths of HPTS, with excitation at 405 nm and emission at 510 nm. The transmembrane anion permeability of vesicles with and without **c5a** was determined by numerically fitting (black lines) the ratio of emission intensities corresponding to the 450 nm/405 nm excitations over the time-lapse. The total anion permeability (ΔP_{x^*}) of each halide ion elicited by **c5a** is shown. (Intensity ratio, F450/F405 = fluorescence emission intensities at excitation wavelengths of 450 nm and 405 nm).

signals, indicating slow exchange between the free and bound forms of $\mathbf{c5a}$ (Supplementary Fig. 6c,d). The signals of free $\mathbf{c5a}$ completely disappeared with ≥ 1 equiv. of the anion and those of the bound $\mathbf{c5a}$ remained. The 1:1 binding ratio is further supported by the HRMS of the mixtures of macrocycle $\mathbf{c5c}$ and all eleven anions (Supplementary Fig. 7). The lower molecular weight of $\mathbf{c5c}$ enabled HRMS to be recorded in the appropriate m/z range of the spectrometer. HRMS revealed the 1:1 complex as the only or dominant species for each anion.

The computationally optimized structures of 1:1 complexes of ${\bf c5}$ with the spherical halides, planar ${\rm NO_3}^-$, tetrahedral ${\rm ClO_4}^-$ and the substituted phosphate ion DPP $^-$ (Fig. 2c), along with ${\rm HSO_4}^-$ and MPP $^-$ (Supplementary Fig. 8) show that iodide is located at the centre of the cavity within the van der Waals contact distances with all endocyclic CH and NH hydrogens, but ${\rm Cl}^-$ or ${\rm Br}^-$ only partially occupies the cavity within the van der Waals contact distances with two CH hydrogens and

two NH hydrogens. With its slightly flexible backbone, macrocycle $\mathbf{c5}$ is also able to accommodate the different shapes of NO $_3^-$, ClO $_4^-$, DPP $^-$, HSO $_4^-$ and MPP $^-$ by having multiple NH···X $^-$ and four CH···X $^-$ interactions with each bound anion.

The binding of **c5a** with eight anions was examined with NMR titration (Table 1). In DMSO-d₆:CDCl₃ (15:85, v/v), titrating **c5a** with each of the three halides caused phenyl protons a to shift downfield (Fig. 3a and Supplementary Fig. 9), but the signal of amide protons b shifts very differently with different halides. This is likely to be due to the competition between DMSO and the halides for hydrogen bonding.

The association constants (K_a) for the binding of **c5a** with the anions were determined by fitting the NMR titration data to a 1:1 binding model using the online fitting tool Bindfit (http://app.supramolecular.org/bindfit/) (Table 1). In DMSO-d₆:CDCl₃ (15:85, v/v, ε = 11), K_a is generally in the range 10^3 – 10^4 M $^{-1}$. In the much more polar CD₃CN:CDCl₃

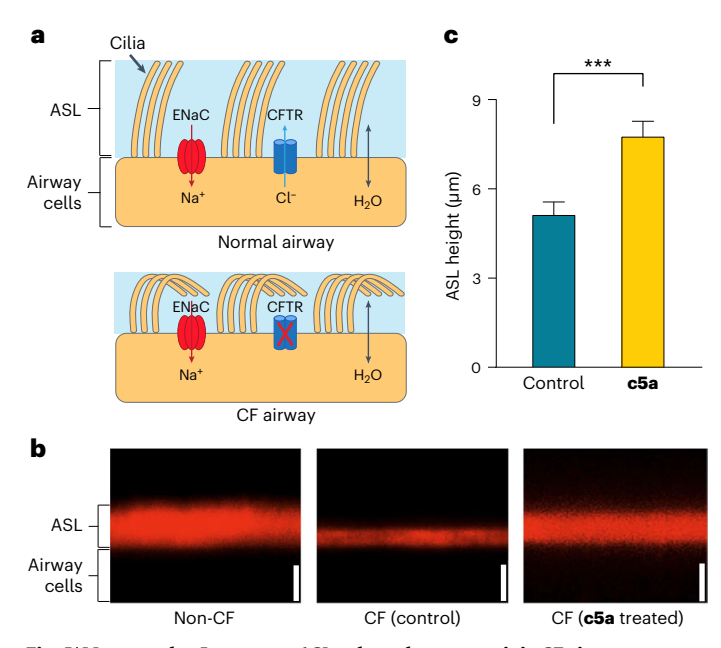


Fig. 5 | **Macrocycle c5a restores ASL volume haemostasis in CF airway epithelial cultures. a**, Illustration of normal and CF human airway cells in profile showing the effect of reduced CFTR-mediated Cl $^-$ secretion combined with unregulated sodium absorption (via epithelial sodium channel or ENaC) on the ASL volume thickness (blue region) 43 . **b**, Representative XZ confocal microscopy images of human airway epithelial cultures (labelled with Texas Red $^-$ dextran, red) showing the steady-state ASL thickness in non-CF (that is, normal) (left) and CF (centre, control) airways and the effect of treating CF cultures with **c5a** (right). The quantitative measurements show that the ASL layer is thickened when the CF cells are treated with **c5a** and that this difference is visible in microscopy images. The location of the unlabelled airway cells is shown for reference. Scale bar, 7 μ m, which shows the length of extended cilia. **c**, Summary of the average thickness of the ASL layers of the control and treated CF cell cultures based on 12 independent measurements (***P < 0.05). Statistical analysis was performed with an unpaired two-sided t-test, P = 0.0005.

 $(80:20, v/v, \varepsilon = 31)$, the K_a values increased by about tenfold, indicating that compared to solvent polarity, the hydrogen-bonding capabilities of the polar solvents (DMSO versus acetonitrile) play a more important role in influencing binding strength. Isothermal titration calorimetry (ITC) experiments revealed that the K_a values in the considerably less polar DMSO:CHCl₃ (5:95, v/v, $\varepsilon = 6.9$) are in fact comparable to those determined in $CD_3CN:CDCl_3$ (80:20, v/v)³³. The K_a values in CH₃CN:CHCl₃ (5:95, v/v, $\varepsilon = 6.4$) from ITC measurements (Supplementary Fig. 10) are over $10^8 \,\mathrm{M}^{-1}$ for $\mathrm{ClO_4}^-$ and $\mathrm{BF_4}^-$ and that for $\mathrm{NO_3}^-$ reaches the 10^9 M⁻¹ range. The high affinity of **c5a** for I⁻ and ClO₄⁻, large and soft anions having low charge density and high polarizability, is apparent. This is probably due to the capabilities of these anions to interact with all the endocyclic CH and NH groups. Besides, the binding of these weakly coordinating and polarizable anions is probably promoted by the five preorganized phenyl CH donors that are characterized by their hydrophobicity and moderate polarizability.

In comparison with cyanostar **iPrCS** that forms 1:1 complexes with anions in CD₃CN:CD₂Cl₂ (1:1, v/v, ε = 23)³⁴, in the more polar CD₃CN:CDCl₃ (80:20, v/v, ε = 31), macrocycle **c5a** binds Cl⁻, Br⁻, BF₄⁻, ClO₄⁻ and lO₄⁻ with affinities 1 to 2 orders of magnitude higher (10⁴ to 10^5 M⁻¹); the K_a values of **c5a** for l⁻ and PF₆⁻ in the more polar solvent are comparable to those of cyanostar **iPrCS**.

NMR titrations of oxoanions HSO_4^- , DPP^- and MPP^- (Fig. 3b, bottom), all being strong hydrogen-bond acceptors³⁵, were also performed (Supplementary Table 1). In DMSO-d₆:CDCl₃ (15:85, v/v), two sets of peaks appeared with \leq 1 equiv. of each of the three anions (Fig. 3b top

and Supplementary Fig. 9), indicating that the free and bound forms of **c5a** undergo slow exchange on the NMR timescale. Direct ^1H NMR titrations in DMSO-d₆:CDCl₃ (70:30, v/v, ε = 34) revealed K_a values over $10^4\,\text{M}^{-1}$ for HSO₄ $^-$ and MPP $^-$ and over $10^3\,\text{M}^{-1}$ for DPP $^-$. K_a values of over $10^4\,\text{M}^{-1}$ were found for both DPP $^-$ and MPP $^-$ in acetone-d₆ with 20% D₂O (ε = 33). Even in acetone-d₆ with 60% D₂O (ε = 56), the binding of **c5b** with DPP $^-$ gave a K_a over $10^3\,\text{M}^{-1}$. In CH₃CN:CHCl₃ (5:95, v/v, ε = 6.4), two-step competition ITC experiments had to be performed to reveal very large K_a values of **c5a** for HSO₄ $^-$ and DPP $^-$ (>10 $^9\,\text{M}^{-1}$) and MPP $^-$ (>10 $^10\,\text{M}^{-1}$). The strong binding of **c5a** with the oxoanions demonstrates that the combination of strong hydrogen-bonding capabilities of the anion guests and multiple hydrogen-bonding interactions, especially those with the convergently placed NH groups, can result in remarkable binding affinity and selectivity.

The affinity of macrocycle **c5** for an anion reflects the binding events involving all endocyclic NH and CH groups, along with other factors such as the attractive ion–dipole interactions between the anion and the amide dipoles and the entropically favourable release of solvent molecules upon binding.

The binding of c5a with the three halides and large, weakly coordinating anions including ClO₄⁻, IO₄⁻ and PF₆⁻ follows a size-dependent trend, with K_a values increasing from Cl⁻ to ClO₄ and then decreasing from ClO₄⁻ to the larger IO₄⁻ and PF₆⁻ (Table 1 and Fig. 3c). This is consistent with reported anion binding of cyanostar **iPrCS**³⁴ and bambusurils³⁶. However, with **c5a**, NO₃ or BF₄ does not follow such a size-dependent trend. Being smaller than I, NO₃ binds to **c5a** with the highest affinity among the anions shown in Table 1 and BF₄, also smaller than I, binds to **c5a** with an affinity similar to I or ClO₄, but higher than the other anions. This observed deviation from size-dependence in the binding of NO_3 or BF_4 to **c5a** was not observed with cyanostars and bambusurils. While the mechanisms remain to be elucidated, the 'abnormal' behaviour of NO₃ or BF₄ indicates the adaptability of **c5a** when binding anions. NO₃⁻, with its planar shape and symmetrically distributed O atoms, is compatible with the cavity of c5a in both shape and hydrogen-bonding pattern; being smaller than I and other larger weakly coordinating anions, BF₄ may engage in more effective ion-dipole interactions with the amide dipoles of **c5a** because of its higher charge density.

The binding of ${\bf c5a}$ with oxoanions ${\sf HSO_4^-}$, ${\sf DPP^-}$ and ${\sf MPP^-}$ deviates further from the size-dependent trend shown by halide ions ${\sf CIO_4^-}$, ${\sf IO_4^-}$ and ${\sf PF_6^-}$ (Fig. 3c and Supplementary Table 1), with much stronger binding affinities in the same solvents and lower sensitivity to the hydrogen-bonding capability of the solvents used. The stronger but less size-dependent binding of ${\bf c5a}$ with oxoanions than with other anions is not observed with known anion binders such as the bambusurils that favour large, weakly coordinating anions.

Direct evidence for the binding of an anion in the cavity of ${\bf c5a}$ was provided by two-dimensional (2D) NMR. The rotating frame Overhause effect spectroscopy (ROESY) spectrum of the 1:1 mixture of ${\bf c5a}$ and MPP $^-$ in DMSO-d $_6$ reveals rotating frame Overhause effects (ROEs) between protons a of ${\bf c5a}$ and protons 1 and 2 of MPP $^-$ (Fig. 3d). By contrast, no significant ROE could be found between protons 1 and 2 of MPP $^-$ and exterior protons d and e of ${\bf c5a}$, confirming that MPP $^-$ is located inside the cavity of ${\bf c5a}$.

Selective halide transport across lipid membranes

The development of strategies for promoting transmembrane anion transport has become an important goal for supramolecular chemistry^{6,37,38}. Although numerous cation carriers, that is cationophores, have been created, effective anionophores have only being developed recently for potential biomedical applications. In particular, diseases such as cystic fibrosis (CF) caused by defective mutations in natural anion channels could benefit from synthetic anionophores that can be used to treat these conditions via 'channel replacement therapy'³⁹. Compared to charged anion carriers that may lead to various complications, neutral anion carriers⁴⁰ are believed to be more beneficial.

Macrocycle **c5a**, a neutral compound with a conformationally defined lipophilic exterior and hydrophilic interior, may partition into biomembranes to facilitate transmembrane anion transport. To examine this possibility, we used a well-established assay based on monitoring the fluorescence of 8-hydroxypyrene-1,3,6-trisulfonic acid (HPTS) entrapped in large unilamellar vesicles (LUVs)⁴¹ to determine the ion transport properties of **c5a**. Upon addition of **c5a**, the collapse of an applied pH gradient resulting from the transport of halide ions was followed using ratiometric fluorescence kinetics (Fig. 4a). As shown in Fig. 4b-d, c5a can indeed transport Cl⁻, Br⁻ and l⁻. The ion permeability elicited by **c5a** (ΔP_{x} -) was further determined by fitting these time-lapse ratiometric fluorescence curves with a quantitative model that included the contributions of association constants 42,43. The corresponding permeability reveals a high transport selectivity for chloride ions with the ratio of Cl⁻:Br⁻:l⁻ = 17.8:1.6:1, a sequence inversely related to the binding affinities of **c5a** for these anions. Such a high transport selectivity, which outperforms those of synthetic Cl⁻ carriers⁴⁴ and even native channels such as the CIC-1 Cl⁻ channel⁴⁵ (with a transport selectivity of Cl⁻:Br⁻:l⁻ = 5:2:1), is quite remarkable.

We also directly measured the anion transport by monitoring the fluorescence of lucigenin encapsulated within LUVs in a halide-free medium at pH 7.0. Halide ions transported into the vesicles would lead to a decrease of lucigenin fluorescence with I^- being the most effective and Cl^- the least effective quencher 46,47 . We found that, in the presence of ${\bf c5a}$, Cl^- resulted in the most reduction of lucigenin fluorescence, followed by Br $^-$ and then I^- (Supplementary Fig. 11), demonstrating that Cl^- is transported much more efficiently than Br $^-$ and I^- with a sequence of $Cl^- > Br^- > I^-$, in agreement with the HPTS assay.

Halide transport by ${\bf c5a}$ (0 to 10 ${\mu}$ M) was further examined by following the fluorescence of intravesicular HPTS with a transmembrane pH gradient. The half-maximal effective concentration (EC50) values derived from dose–response curves are 0.31 ${\mu}$ M for Cl⁻, 4.11 ${\mu}$ M for Br⁻ and »10 ${\mu}$ M for I⁻ (too large to be measured due to the low transport activity of I⁻) (Supplementary Fig. 12). These EC50 values provide another independent piece of evidence for anion transport selectivity and the highly efficient transport of Cl⁻. The transmembrane ion transport mediated by **c5a** in the presence of LiCl, NaCl, KCl or RbCl shows negligible differences, indicating that **c5a** is indeed an anion transporter (Supplementary Fig. 13)⁴¹.

The anion selectivity sequence of **c5a** does not follow the Hofmeister order⁴⁸, which is remarkable but has been documented with some other synthetic transporters^{44,49}. Although the resolution of the underlying mechanism for this phenomenon requires additional detailed studies, the observed selectivity, which seems to be proportional to the hydrogen-bonding ability of the halides, may be qualitatively rationalized based on the notion that the strongest binders may not be the best transporters⁴³. Among the three halides, iodide binds with the highest affinity. This could impede its release from the complex, leading to the lowest transport efficiency.

Since macrocycle **c5a** has a low propensity for self-aggregation, the cross-bilayer anion transport is unlikely to be mediated by membrane-spanning pores or channels that would require a tubular stacking of multiple molecules of **c5a**. It is therefore reasonable to hypothesize that **c5a** mediates halide transport as a carrier. This hypothesis was validated by an assay using dipalmitoylphosphatidylcholine (DPPC) vesicles. DPPC bilayers undergo gel-to-fluid phase transitions at 41 °C (ref. 50). Below this temperature, the bilayer is in the gel phase in which c5a could not operate as a carrier. Again, using the HPTS fluorescence as an indicator, chloride transport was completely prohibited at 25 °C and when the temperature was raised to 45 °C, enhanced halide transport was measured in the presence of **c5a** (Supplementary Fig. 14). These results indicate that the mobility of c5a within the lipid bilayer must have played a critical role in transmembrane transport, that is macrocycle c5a serves as a carrier that ferries the anions across the lipid bilayers.

Restoration of airway surface liquid of CF cells

Efficient and selective transport of Cl $^-$ across the cell membrane is biologically and medically significant 6,37,38 . Natural chloride channels are known to be responsible for a broad range of functions, with a large spectrum of diseases being caused by defective Cl $^-$ channels 51 . Facilitating the efficient and selective Cl $^-$ transport across lipid membranes, macrocycles $\mathbf{c5}$ offer the possibility to remedy malfunctioning anion transport in a variety of diseases 51 . Among these, cystic fibrosis (CF) is an extensively studied, life-shortening disease caused by the impaired functions of CF transmembrane conductance regulator protein (CFTR), an anion channel, owing to various mutations in the CFTR gene. In the lung, this leads to the dehydration and acidification of the airway surface liquid (ASL), a thin layer of fluid covering the luminal (apical) surface of the airway epithelium (Fig. 5a) 52 , causing hyper-concentration of mucin biopolymers and increased mucus viscoelasticity 43 . This impairs the cilia beating frequency 53 and reduces mucociliary transport rates 54 .

To test this intriguing possibility, we cultured human bronchial epithelial (HBE) cells isolated from CF patients at the time of lung transplant as a model system for diseased airways. These cells were cultured on permeable supports and studied after full differentiation (~21 days). Compound c5a was then apically applied daily. After five days, the thickness of the fluorescently labelled ASL layer⁵⁵ on the surface of the HBE cell layer was measured using XZ confocal scanning microscopy (Fig. 5b). Compared with the reduced ASL thickness associated with CF cultures, the ASL layer was visibly thickened when the CF cells were treated with c5a. Quantitative measurements (Fig. 5c) show that the ASL thickness is increased by more than 50%: $7.8 \pm 1.7 \, \mu m$ when treated with **c5a** versus 5.1 ± 1.4 µm with the control CF cells. Therefore, c5a successfully restored the hydration and the volume of the ASL by rectifying the malfunctioning chloride transport in these cells, which is a key objective of therapeutic interventions for CF. The performance of macrocycle c5a is comparable to, if not better than, that in the landmark work reported by Burke and co-workers under similar conditions⁵⁶.

Conclusions

Star-shaped pentaamide macrocycles **c5a-c** were synthesized from the one-pot reaction of the corresponding monomers. The efficient, scalable synthetic procedure allows derivatives of macrocycles c5 to be prepared with ready structural modification, enabling efficient structural tuning and functional optimization. These macrocycles share a fully constrained backbone that locks endocyclic NH and CH groups into a convergent arrangement, leading to high-affinity binding of halides, large anions and oxoanions. Examining the binding affinities of **c5** for halide ions and weakly coordinating anions reveals size-dependent recognition favouring large anions, while the complexation of oxoanions shows that anions with strong hydrogen-bonding capabilities achieve remarkable binding affinities, even in solvents containing high proportions of water. The exceptional anion binding capabilities of macrocycles c5 can be attributed to the presence of the preorganized endocyclic amide NH and phenyl CH groups. As powerful hydrogen-bond donors, the NH donors form multiple, strong hydrogen bonds with oxoanions that are known to be strong hydrogen-bond acceptors. The five convergently placed, hydrophobic and moderately polarizable phenyl CH groups favour large, polarizable anions capable of interacting with most or all CH and NH groups. These distinct interactions, along with the five inwardly pointing amide dipoles, result in the unique, versatile anion binding behaviour shown by macrocycles c5. The ready insertion of macrocycles c5 equipped with hydrophobic side chains into lipid bilayers enables efficient transmembrane chloride transport with a selectivity even higher than synthetic and natural chloride transporters. The apical application of c5a to CF cell cultures also successfully restored the ASL, demonstrating the potential of these compounds as therapeutic agents for treating diseases related to anion transport. As these molecules are expected to be immune

tolerant, more effective therapeutics might be developed that may circumvent some of the limitations seen with biomacromolecules. Based on this structurally tunable platform, the development of the next-generation anion binders, transporters and potential therapeutics for channel-related diseases can be envisioned.

Online content

Any methods, additional references, Nature Portfolio reporting summaries, source data, extended data, supplementary information, acknowledgements, peer review information; details of author contributions and competing interests; and statements of data and code availability are available at https://doi.org/10.1038/s41557-023-01315-w.

References

- Whitty, A. Cooperativity and biological complexity. Nat. Chem. Biol. 4, 435–439 (2008).
- Zhou, Y., Morais-Cabral, J. H., Kaufman, A. & MacKinnon, R. Chemistry of ion coordination and hydration revealed by a K⁺ channel–Fab complex at 2.0 Å resolution. *Nature* 414, 43–48 (2001).
- Sui, H. X., Han, B. G., Lee, J. K., Walian, P. & Jap, B. K. Structural basis of water-specific transport through the AQP1 water channel. Nature 414, 872–878 (2001).
- Dutzler, R., Campbell, E. B., Cadene, M., Chait, B. T. & MacKinnon, R. X-ray structure of a ClC chloride channel at 3.0 Å reveals the molecular basis of anion selectivity. *Nature* 415, 287–294 (2002).
- Pflugrath, J. W. & Quiocho, F. A. Sulphate sequestered in the sulphate-binding protein of Salmonella typhimurium is bound solely by hydrogen bonds. Nature 314, 257–260 (1985).
- Wu, X., Gilchrist, A. M. & Gale, P. A. Prospects and challenges in anion recognition and transport. Chem 6, 1296–1309 (2020).
- Sessler, J. L., Gale, P. A. & Cho, W.-S. Anion Receptor Chemistry (RSC Publishing, 2006).
- John, E. A., Massena, C. J. & Berryman, O. B. Helical anion foldamers in solution. Chem. Rev. 120, 2759–2782 (2020).
- Borissov, A. et al. Anion recognition in water by charge-neutral halogen and chalcogen bonding foldamer receptors. J. Am. Chem. Soc. 141, 4119–4129 (2019).
- Rebek, J. Jr. Model studies in molecular recognition. Science 235, 1478–1484 (1987).
- Gong, B. et al. Creating nanocavities of tunable sizes: Hollow helices. Proc. Natl Acad. Sci. USA 99, 11583–11588 (2002).
- Jiang, H., Léger, J. M. & Huc, I. Aromatic δ-peptides. J. Am. Chem. Soc. 125, 3448–3449 (2003).
- Höger, S. Shape-persistent macrocycles: from molecules to materials. Chem. Eur. J. 10, 1320–1329 (2004).
- Guieu, S., Crane, A. K. & MacLachlan, M. J. Campestarenes: novel shape-persistent Schiff base macrocycles. *Chem. Commun.* 47, 1169–1171 (2011).
- Qin, B. et al. Crystallographic evidence of an unusual, pentagon-shaped folding pattern in a circular aromatic pentamer. Org. Lett. 10, 5127–5130 (2008).
- Lee, S. M., Chen, C. H. & Flood, A. H. A pentagonal cyanostar macrocycle with cyanostilbene CH donors binds anions and forms dialkylphosphate [3]rotaxanes. *Nat. Chem.* 5, 704–710 (2013).
- 17. Li, Y. & Flood, A. H. Pure C—H hydrogen bonding to chloride ions: a preorganized and rigid macrocyclic receptor. *Angew. Chem. Int. Ed.* **47**, 2649–2652 (2008).
- Bisson, A. P., Lynch, V. M., Monahan, M.-K. C. & Anslyn, E. V. Recognition of anions through NH—π hydrogen bonds in a bicyclic cyclophane—selectivity for nitrate. *Angew. Chem. Int. Ed. Engl.* 36, 2340–2342 (1997).
- Sessler, J. L. & Davis, J. M. Sapphyrins: versatile anion binding agents. Acc. Chem. Res. 34, 989–997 (2001).

- 20. Brooks, S. J., Gale, P. A. & Light, M. E. Anion-binding modes in a macrocyclic amidourea. *Chem. Commun.* **41**, 4344–4346 (2006).
- Tresca, B. W. et al. Substituent effects in CH hydrogen bond interactions: linear free energy relationships and influence of anions. J. Am. Chem. Soc. 137, 14959–14967 (2015).
- 22. Bondy, C. R. & Loeb, S. J. Amide based receptors for anions. Coord. Chem. Rev. **240**, 77–99 (2003).
- Kang, S. O., Begum, R. A. & Bowman-James, K. Amide-based ligands for anion coordination. *Angew. Chem. Int. Ed.* 45, 7882–7894 (2006).
- Choi, K. H. & Hamilton, A. D. Macrocyclic anion receptors based on directed hydrogen bonding interactions. *Coord. Chem. Rev.* 240, 101–110 (2003).
- Choi, K. H. & Hamilton, A. D. Selective anion binding by a macrocycle with convergent hydrogen bonding functionality. J. Am. Chem. Soc. 123, 2456–2457 (2001).
- Yuan, L. H. et al. Highly efficient, one-step macrocyclizations assisted by the folding and preorganization of precursor oligomers. J. Am. Chem. Soc. 126, 11120–11121 (2004).
- Cao, R. K., Rossdeutcher, R. B., Wu, X. X. & Gong, B.
 Oligo(5-amino-N-acylanthranilic acids): amide bond formation
 without coupling reagent and folding upon binding anions. Org.
 Lett. 22, 7496–7501 (2020).
- 28. Juwarker, H. & Jeong, K. S. Anion-controlled foldamers. *Chem. Soc. Rev.* **39**, 3664–3674 (2010).
- 29. Hua, Y., Liu, Y., Chen, C.-H. & Flood, A. H. Hydrophobic collapse of foldamer capsules drives picomolar-level chloride binding in aqueous acetonitrile solutions. *J. Am. Chem.* Soc. **135**, 14401–14412 (2013).
- Chang, K. J., Kang, B. N., Lee, M. H. & Jeong, K. S. Oligoindole-based foldamers with a helical conformation induced by chloride. J. Am. Chem. Soc. 127, 12214–12215 (2005).
- 31. Juwarker, H. et al. Anion binding of short, flexible aryl triazole oligomers. J. Org. Chem. **74**, 8924–8934 (2009).
- 32. Helttunen, K. R. et al. Oligoamide foldamers as helical chloride receptors—the influence of electron-withdrawing substituents on anion-binding interactions. *Chem. Asian J.* **14**, 647–654 (2019).
- 33. Liu, Y., Sengupta, A., Raghavachari, K. & Flood, A. H. Anion binding in solution: beyond the electrostatic regime. *Chem* **3**, 411–427 (2017).
- Qiao, B., Anderson, J. R., Pink, M. & Flood, A. H. Size-matched recognition of large anions by cyanostar macrocycles is saved when solvent-bias is avoided. *Chem. Commun.* 52, 8683–8686 (2016).
- 35. Pike, S. J., Hutchinson, J. J. & Hunter, C. A. H-bond acceptor parameters of anions. *J. Am. Chem. Soc.* **39**, 6700–6706 (2017).
- Yawer, M. A., Havel, V. & Sindelar, V. A bambusuril macrocycle that binds anions in water with high affinity and selectivity. *Angew*. *Chem. Int. Ed.* 54, 276–279 (2015).
- Davis, A. P., Sheppard, D. N. & Smith, B. D. Development of synthetic membrane transporters for anions. *Chem. Soc. Rev.* 36, 348–357 (2007).
- 38. Gokel, G. W. & Negin, S. Synthetic ion channels: from pores to biological applications. Acc. Chem. Res. 46, 2824–2833 (2013).
- Tomich, M., Bukovnik, U., Layman, J. & Schultz, B. D. Channel replacement therapy for cystic fibrosis. in Cystic Fibrosis -Renewed Hopes through Research (ed Sriramulu, D.) 291–332 (InTech, 2012).
- 40. Valkenier et al. Lipophilic balance a new design principle for transmembrane anion carriers. *Chem. Sci.* **5**, 1128–1134 (2014).
- Sakai, N. & Matile, S. The determination of the ion selectivity of synthetic ion channels and pores in vesicles. *J. Phys. Org. Chem.* 19, 452–460 (2006).
- 42. Shen, Y. et al. Ultrasensitive liposome-based assay for the quantification of fundamental ion channel properties. *Anal. Chim. Acta* **1112**, 8–15 (2020).

- Matsui, H. et al. Evidence for periciliary liquid layer depletion, not abnormal ion composition, in the pathogenesis of cystic fibrosis airways disease. Cell 5, 1005–1015 (1998).
- Jentzsch, A. V. et al. Transmembrane anion transport mediated by halogen-bond donors. Nat. Commun. 3, 905 (2012).
- Rychkov, G. Y., Pusch, M., Roberts, M. L., Jentsch, T. J. & Bretag, A. H. Permeation and block of the skeletal muscle chloride channel, ClC-1, by foreign anions. J. Gen. Physiol. 111, 653–665 (1991).
- Biwersi, J., Tulk, B. & Verkman, A. S. Long-wavelength chloride-sensitive fluorescent indicators. *Anal. Biochem.* 219, 139–143 (1994).
- Seganish, J. L., Fettinger, J. C. & Davis, J. T. Facilitated chloride transport across phosphatidylcholine bilayers by an acyclic calixarene derivative: structure-function relationships. Supramol. Chem. 18, 257–264 (2006).
- 48. Kunz, W., Nostro, P. L. & Ninham, B. W. The present state of affairs with Hofmeister effects. *Curr. Opin. Colloid Interface Sci.* **9**, 1–18 (2004).
- Behera, H. & Madhavan, N. Anion-selective cholesterol decorated macrocyclic transmembrane ion carriers. J. Am. Chem. Soc. 139, 12919–12922 (2017).
- 50. Behr, J.-P., Kirch, M. & Lehn, J.-M. Carrier-mediated transport through bulk liquid membranes: dependence of transport rates and selectivity on carrier properties in a diffusion-limited process. *J. Am. Chem.* Soc. **107**, 241–246 (1985).

- Jentsch, T. J., Maritzen, T. & Zdebik, A. A. Chloride channel diseases resulting from impaired transepithelial transport or vesicular function. J. Clin. Invest. 115, 2039–2046 (2005).
- 52. Haq, I. J., Gray, M. A., Garnett, J. P., Ward, C. & Brodlie, M. Airway surface liquid homeostasis in cystic fibrosis: pathophysiology and therapeutic targets. *Thorax* 71, 284–287 (2016).
- 53. Alikadic, S. et al. Ciliary beat frequency in nasal and bronchial epithelial cells in patients with cystic fibrosis. *Eur. Respir. J.* **38**, 4550 (2011).
- Anderson, W. H. et al. The relationship of mucus concentration (hydration) to mucus osmotic pressure and transport in chronic bronchitis. Am. J. Respir. Crit. Care Med. 192, 182–190 (2015).
- 55. Goralski, J. L., Wu, D., Thelin, W. R., Boucher, R. C. & Button, B. The *in vitro* effect of nebulised hypertonic saline on human bronchial epithelium. *Eur. Respir. J.* **51**, 1702652 (2018).
- Muraglia, K. A. et al. Small-molecule ion channels increase host defences in cystic fibrosis airway epithelia. *Nature* 567, 405–408 (2019).
- te Velde, G. et al. Chemistry with ADF. J. Comput. Chem. 22, 931–967 (2001).

Publisher's note Springer Nature remains neutral with regard to jurisdictional claims in published maps and institutional affiliations.

© The Author(s), under exclusive licence to Springer Nature Limited 2023

Methods

Materials and instruments

Chemicals were purchased from commercial sources and used as received. Silica gel for analytical thin-layer chromatography (TLC) and column chromatography (mesh 230–400) was purchased from Sorbent Technologies. 1H NMR spectra were recorded at 400 MHz on a Varian Inova-400 and at 500 MHz on a Varian Inova-500. ^{13}C NMR spectra were recorded at 75 MHz on a Varian Mercury-300 spectrometer at ambient temperature using CDCl $_3$ or DMSO-d $_6$ as solvents (Cambridge Isotope Laboratories). Chemical shifts are reported in parts per million (ppm) downfield from tetramethylsilane or residual of deuterated solvents. Coupling constants in 1H NMR are expressed in Hertz (Hz). High-resolution electrospray ionization mass spectrometry (HRMS-ESI) was recorded on a Bruker SolariX 12 T Fourier Transform Mass Spectrometer. An Agilent 6530 Q-TOF LC/MS was used to collect mass spectra of the complexes between ${\bf c5c}$ and anions in negative ion mode.

Unless otherwise specified, all solvents, including high-boiling-point solvents, were removed under reduced pressure with a rotary evaporator. Anhydrous toluene was used for the coupling reactions.

Isothermal titration calorimetry (ITC) experiments were performed using a MicroCal VP-ITC. ITC experiments were conducted by adding -1.5 ml of a solution containing **c5a** to the sample cell. This was followed by titrating 10 μ l aliquots of a solution containing the corresponding TBA–X salt (-10–14× concentration of **c5a** solution) from the syringe into the sample cell. Heats of dilution were obtained by titrating 10 μ l aliquots of the TBA–X solution from the syringe into the sample cell in the absence of **c5a**. The heats of dilution of the anion salts (TBA–X) were subtracted from the overall heats for titrating the anion salts into **c5a**. ITC data processing and curve fitting was done using the Origin program (MicroCal).

Preparation of 4-(N,N-dimethylamino) pyridine salt

4-(*N*,*N*-Dimethylamino)pyridine hydrochloride (DMAP·HCl)⁵⁸ and 4-(*N*,*N*-dimethylamino)pyridine hydrobromide (DMAP·HBr)⁵⁹ were synthesized using the published method without any modification. For the synthesis of 4-(*N*,*N*-dimethylamino)pyridine hydroiodide (DMAP·Hl), DMAP·HCl and KI (2.0 equiv.) were dissolved in acetone. The white solid KCl formed and was filtered off. The resulting solution was dried under reduced pressure to afford the crude DMAP·Hl salt. Further purification of DMAP·Hl salt was done by dissolving the crude product in hot toluene and filtering off any insoluble solid. The filtrate was concentrated to afford the DMAP·Hl salt.

Hydrogenation reaction

The reduction of each nitro compound to its corresponding amine was carried out in a mixed solvent of 20% methanol and 80% dichloromethane, in the presence of a catalytic amount of Pd/C and pressurized hydrogen gas. For the reduction of the nitro group in the benzoxazinone residue, CH_2Cl_2 was used as a solvent as methanol could react with the benzoxazinone residue to afford the corresponding methyl ester. The resulting reaction solution was stirred at room temperature for 2–8 h. Upon the completion of the reduction reaction, developed TLC plates were stained with a solution of ninhydrin in ethanol and the spot of aromatic amine always changed colour from red to purple. Pd/C was then filtered off and the filtrate was concentrated to afford the corresponding amine that was pure enough to be applied directly to the coupling reaction without any further purification. No analytical data are available for aromatic amines, as they were typically considered to be unstable under the ambient environment.

¹H NMR titration methods

Titrations of **c5a** and **c5b** with anions as their tetra-n-butylammonium (TBA), tetraethylammonium (TEA) and tetramethylammonium (TMA) salts were carried out using 1 H NMR (400 MHz) at 25 $^{\circ}$ C. First, 0.4 ml of the corresponding host solutions was prepared in rubber-capped NMR

tubes. Aliquots of concentrated guest solution containing the hosts were added to the NMR tubes using a 20 μ l pipette. An initial 1H NMR spectrum was collected and additional spectra were obtained after each injection of guest solution. All titration 1H NMR spectra were stacked together and the chemical shifts of the internal aromatic CH proton were then fitted to a 1:1 binding model using BindFit v0.5 (http://app.supramolecular.org/bindfit/) to evaluate the binding constants to anions.

One-pot synthesis of macrocycles c5

The one-pot synthesis of **c5a** was probed using the ring-opening reaction of benzoxazinone monomer **2a** (Fig. 1b and Supplementary Scheme 2). In toluene, while heating **2a** (2 mM) and DMAP·HCl and DMAP·HI under reflux led to **c5a** in 5 and 0% yields, respectively, treating **2a** and DMAP·HBr (40 mol%) under the same conditions gave **c5a** in 27% yield, indicating that Br¯ served as a template for one-pot cyclization. Replacing DMAP·HBr with the 1:1 mixture of diphenyl phosphate (DPP) and DMAP (40 mol%) significantly improved the yield (-45%) of **c5a**, suggesting that DPP¯ is a more effective template than Br¯. Based on the same one-pot procedure, macrocycles **c5b** and **c5c**, which carry sidechains having tri(ethylene glycol) (Tg) and allyl tails, for enhanced solubility and further modification, respectively, were synthesized from monomers **2b** and **2c** in yields of 38 and 39%.

UV-vis titration methods

The host solution of **c5a** (20 μ M) was prepared in CH₃OH:CHCl₃ (5:95, v/v). The solution of guests (50 equiv.) being studied was prepared in the host solutions in order to avoid any dilution effect during the titration procedure. Aliquots of guest solution were added to the host solution in a spectrometric cell. The UV–vis spectra were collected on a Beckman Coulter DU 800 spectrophotometer at room temperature.

Competition NMR experiments for determining the K_a values of slow-exchange oxoanions

Interaction between **c5a** and acetate, DPP $^-$ or MPP $^-$ ('anion') is in slow-exchange on the NMR timescale. In the presence of Cl $^-$ as the competitor, fast exchange occurred in the NMR titrations, which allowed the K_a of the complex between **c5a** and each of these anions to be determined.

In the NMR titration experiment, the solution of an anion of interest was gradually added to the solution containing **c5a** (0.5 mM) and TBA•Cl (100 mM), the competitor, resulting in the signal of proton a of **c5a** to shift in the ¹H NMR spectrum. The change in chemical shifts was due to the formation of complex **c5a**•anion that is more stable than complex **c5a**•Cl

$$Cl^- + \mathbf{c}5\mathbf{a} \cdot Cl^- + \text{anion} \longrightarrow Cl^- + \mathbf{c}5\mathbf{a} \cdot \text{anion}$$

Since the chloride ion is in large excess, the concentration of free chloride, $[Cl^-]$, can be regarded as being unchanged (constant) before and after titrating with the anion.

The titration data can be fitted to a 1:1 binding isotherm to obtain K_a (relative)³⁶

$$K_{a}(\text{relative}) = \frac{[\textbf{c5a} \cdot \text{anion}]}{[\textbf{c5a} \cdot \text{Cl}^{-}] \times [\text{anion}]} = \frac{K_{a}}{K_{a(\text{Cl}^{-})} \times [\text{Cl}^{-}]}$$

Where

$$K_{\rm a} = \frac{[{\bf c}5{\bf a} \cdot {\rm anion}]}{[{\bf c}5{\bf a}] \times [{\rm anion}]}$$

$$K_{a(Cl^{-})} = \frac{[c5a \cdot Cl^{-}]}{[c5a] \times [Cl^{-}]}$$
 (association constant between c5a and Cl⁻)

Since the binding constant of **c5a** with Cl⁻ ($K_{a(Cl^-)}$) is measured by direct NMR titration, the binding constant of **c5a** with

the slow-exchange oxoanions is then calculated based on the following equation

 $K_{a} = K_{a}(\text{relative}) \times K_{a(Cl^{-})} \times [Cl^{-}]$

Two-step competition ITC experiments for determining the K_a of c5a and iodide

In CH₃CN:CHCl₃ (5:95, v/v), the binding affinity of **c5a** for Γ was too high to be determined with direct NMR or ITC titration. Instead, two-step competition ITC experiments with Cl⁻ as the competitor were performed. Titrating macrocycle **c5a** (0.5 mM) with TBA·I (5.0 mM) in the presence of TBA·Cl (2.5 mM) gave K (relative), which, along with K (Cl⁻), yielded the K₀ of **c5a** and Γ .

¹H NMR signals of macrocycles c5a-c in different solvents

The 1 H NMR spectra of macrocycles ${\bf c5a-c}$ in CDCl $_3$ (0.2 mM) reveal dispersed or discernible resonances (Supplementary Fig. 15), indicating the limited self-aggregation of these compounds as suggested by the crystal structures. In CDCl $_3$ with 1 to 100% (v/v) DMSO-d $_6$, the NMR signals of ${\bf c5a}$ (1 mM) are well dispersed, with the resonance of sidechain amide protons c showing an upfield shift of 0.5 ppm, backbone amide protons b exhibiting a large downfield shift of 1.41 ppm and that of the endocyclic CH proton a experiencing a very small downfield shift of 0.06 ppm (Supplementary Fig. 16). These observations demonstrate that amide protons b are exposed to solvent while endocyclic phenyl protons a have minimal, if any, interaction with DMSO.

Binding stoichiometry and affinity revealed by UV, NMR and ITC

The linear dependence of the UV–vis absorbance of **c5a** changed (Fig. 2a) abruptly (at 330 nm) at 1 equiv. of tetrabutylammonium chloride (TBA $^+$ Cl $^-$), which is consistent with the 1:1 binding between **c5a** and Cl $^-$. Titrating **c5a** with the other anions revealed the same abrupt changes in absorbance around 330 nm at 1 equiv. of each anion (Supplementary Fig. 5), indicating that **c5a** binds with the anions in a 1:1 ratio.

In DMSO- d_6 :CDCl₃ (15:85, v/v), titrating **c5a** with each of the three halides caused phenyl protons a to shift downfield by 0.20 ppm with Cl⁻, 0.13 ppm with Br⁻ or 0.43 ppm with I⁻ (Fig. 3a, top and Supplementary Fig. 9). Compared with protons a, the signal of amide protons b shifts very differently (Fig. 3a and Supplementary Fig. 9). Cl⁻ induces a small (0.08 ppm) downfield shift, while Br⁻ causes a minuscule (-0.02 ppm) and I^- a much larger (-0.57 ppm)upfield shift. The shifts of protons b induced by different halides are likely to be due to the competition between DMSO and the halides for hydrogen bonding. Binding a halide to **c5a** expels the DMSO molecules from the cavity (Fig. 3a, bottom). Binding Cl⁻ leads to stronger hydrogen-bonding strength 'felt' by protons b, causing the ¹H resonance to shift further downfield. On the other hand, displacing DMSO by Br⁻ and especially I⁻, as weaker hydrogen-bond acceptors⁴, results in reduced hydrogen-bonding strengths sensed by protons b, leading to upfield shifts.

NMR titrations of oxoanions HSO₄⁻, DPP⁻ and MPP⁻ (Fig. 3b, bottom) were performed in different solvents as presented under. In DMSO-d₆:CDCl₃ (15:85, v/v), titrating **c5a** with the TBA⁺ salt of HSO₄⁻ or MPP⁻ or the tetramethylammonium (TMA⁺) salt of DPP⁻ revealed that the free and bound forms of **c5a** undergo slow exchange on the NMR timescale. Direct ¹H NMR titrations performed in DMSO-d₆:CDCl₃ (70:30, v/v, ε = 34) gave K_a values over 10^4 M⁻¹ for HSO₄⁻ and MPP⁻ and over 10^3 M⁻¹ for DPP (Supplementary Table 1); in acetone-d₆ with 20% D₂O (ε = 33), both DPP⁻ and MPP⁻ show binding affinities for **c5a** in the 10^4 M⁻¹ range; in acetone-d₆ with 60% D₂O (ε = 56), DPP⁻ still binds with **c5b** with a K_a over 10^3 M⁻¹ (Supplementary Fig. 17); and in the much less polar CH₃CN:CHCl₃ (5:95, v/v, ε = 6.4), the K_a values for the binding of **c5a** with the three oxoanions had to be determined with two-step

competition ITC experiments, with K_a values for HSO₄⁻ and DPP⁻ being over $10^9 \,\mathrm{M}^{-1}$ and that of MPP⁻ is over $10^{10} \,\mathrm{M}^{-1}$ (Supplementary Table 1).

Other information and additional data

See the Supplementary Information for experimental procedures and conditions including synthesis, assays for vesicle-based assays for transmembrane halide transport, methods for CF cell culturing and confocal imaging studies and analytical data from ¹H, ¹³C and 2D NMR spectroscopy, mass spectrometry, NMR and ITC titration and the crystallography data for **c5a**. The structure of **c5a** is too disordered for the crystallographic data to be deposited with the CCDC. An ORTEP-style illustration of the crystal structure of **c5a** with 30% probability ellipsoids is included (Supplementary Fig. 19).

Reporting summary

Further information on research design is available in the Nature Portfolio Reporting Summary linked to this article.

Data availability

Single-crystal X-ray structure data for macrocycle **c5c** (CCDC reference number: 2124841) can be obtained free of charge from the Cambridge Crystallographic Data Centre at www.ccdc.cam.ac.uk/data_request/cif. The source data for Supplementary Figs. 1, 2, 5, 6a,b, 10–14, 17 and 18 can be obtained free of charge from Figshare at https://doi.org/10.6084/m9.figshare.23302427 (ref. 60). Source data are provided with this paper.

Code availability

The codes used in the calculations of data from vesicle-based halide transport HPTS assays can be obtained free of charge from Figshare at https://doi.org/10.6084/m9.figshare.23302427 (ref. 60).

References

- Liu, Z. H., Ma, Q. Q., Liu, Y. X. & Wang, Q. M.
 4-(N,N-Dimethylamino)pyridine hydrochloride as a recyclable catalyst for acylation of inert alcohols: substrate scope and reaction mechanism. Org. Lett. 16, 236–239 (2014).
- Zhang, Z. G. et al. Efficient synthesis of cyclic carnonates from atmospheric CO₂ using a positive charge delocalized ionic liquid catalyst. ACS Sustain. Chem. Eng. 5, 2841–2846 (2017).
- Cao, R. et al. Aromatic pentaamide macrocycles bind anions with high-affinity for transport across biomembranes. *Figshare* https:// doi.org/10.6084/m9.figshare.23302427 (2023).
- Gong, B. Linear and cyclic aromatic oligoamides, methods of making same and uses thereof. US patent PCT/US2021/050041 (2021).

Acknowledgements

We acknowledge support from the US National Science Foundation (CHE-2304878 to B.G. for the conceptualization, design, data collection, analysis, decision to publish or preparation of the manuscript; CHE-1905094 and 2108538 to B.G. for preparing some of the synthetic building blocks; and CHE-2108597 to D.P.M. for the computational studies) for financial support; the Cystic Fibrosis Foundation (BUTTON19G0) and the NIH (R01HL125280) to B.B. for assessing the effect of c5a on restoring the ASL of cultured CF cells; the National Key R&D Program of China (2020YFA0908100), the NSFC (81627801) and the K. C. Wong Education Foundation (Hong Kong) to Z.S. for the design and performance of experiments on anion transport, for the determination of transport selectivity and for the preparation of the manuscript; and the Rabinowitz Honors College Research Assistant Program and a Lister Endowed Fellowship from Hofstra University (to D.P.M.). The funders had no role in study design, data collection and analysis, decision to publish or preparation of the manuscript. Computations were carried out at the Center

for Computational Research at the University at Buffalo (http://hdl. handle.net/10477/79221).

Author contributions

R.C. and R.B.R. designed and conducted the syntheses and also performed the binding studies. T.A.S. performed ITC experiments. Y.S., Y.Z., R.B.R. and Z.S. performed the vesicle-based assays on anion transport. X.W. processed the X-ray data. D.P.M., L.S.B., K.R. and E.Z. performed the computational studies. B.B designed and, along with M.I.G. and M.F.F., performed experiments on cystic fibrosis cell cultures. T.S. helped with the NMR experiments. B.G. conceived and supervised the project. Z.S. and B.G. co-wrote the paper. All authors participated in discussion and editing of the manuscript.

Competing interests

A provisional US patent application (PCT/US2021/050041) regarding the synthesis, anion binding, anion transport and potential therapeutic

uses involving macrocycles **c5** has been filed⁶¹. The remaining authors declare no competing interests.

Additional information

Supplementary information The online version contains supplementary material available at https://doi.org/10.1038/s41557-023-01315-w.

Correspondence and requests for materials should be addressed to Zhifeng Shao or Bing Gong.

Peer review information *Nature Chemistry* thanks Maija Nissinen and the other, anonymous, reviewer(s) for their contribution to the peer review of this work.

Reprints and permissions information is available at www.nature.com/reprints.

nature portfolio

Corresponding author(s):	Zhifeng Shao, Bing Gong
Last updated by author(s):	Jun 10, 2023

Reporting Summary

Nature Portfolio wishes to improve the reproducibility of the work that we publish. This form provides structure for consistency and transparency in reporting. For further information on Nature Portfolio policies, see our <u>Editorial Policies</u> and the <u>Editorial Policy Checklist</u>.

<u> </u>				
St	- a	tic	:ti	2

For	all statistical analyses, confirm that the following items are present in the figure legend, table legend, main text, or Methods section.
n/a	Confirmed
	The exact sample size (n) for each experimental group/condition, given as a discrete number and unit of measurement
	A statement on whether measurements were taken from distinct samples or whether the same sample was measured repeatedly
	The statistical test(s) used AND whether they are one- or two-sided Only common tests should be described solely by name; describe more complex techniques in the Methods section.
\boxtimes	A description of all covariates tested
\boxtimes	A description of any assumptions or corrections, such as tests of normality and adjustment for multiple comparisons
	A full description of the statistical parameters including central tendency (e.g. means) or other basic estimates (e.g. regression coefficient) AND variation (e.g. standard deviation) or associated estimates of uncertainty (e.g. confidence intervals)
	For null hypothesis testing, the test statistic (e.g. <i>F</i> , <i>t</i> , <i>r</i>) with confidence intervals, effect sizes, degrees of freedom and <i>P</i> value noted Give <i>P</i> values as exact values whenever suitable.
\times	For Bayesian analysis, information on the choice of priors and Markov chain Monte Carlo settings
\boxtimes	For hierarchical and complex designs, identification of the appropriate level for tests and full reporting of outcomes
\times	Estimates of effect sizes (e.g. Cohen's d, Pearson's r), indicating how they were calculated
	Our web collection on <u>statistics for biologists</u> contains articles on many of the points above.
C 0:	ftware and code

Software and code

Policy information about availability of computer code

Data collection

Microsoft Excel Software (2019) is used for data presenting and processing. ADF software package were used for density functional theory calculations. XZ confocal images under each condition was processed using the custom MATLAB code to generate ASL high thickness.

Data analysis

For each condition, the above-noted MATLAB code exported ASL height data to a Microsoft Excel file for plotting and subsequent analysis. The custom MATLAB codes have been deposited at http://doi.org/10.6084/m9.figshare.23302427.

For manuscripts utilizing custom algorithms or software that are central to the research but not yet described in published literature, software must be made available to editors and reviewers. We strongly encourage code deposition in a community repository (e.g. GitHub). See the Nature Portfolio guidelines for submitting code & software for further information.

Data

Policy information about availability of data

All manuscripts must include a data availability statement. This statement should provide the following information, where applicable:

- Accession codes, unique identifiers, or web links for publicly available datasets
- A description of any restrictions on data availability
- For clinical datasets or third party data, please ensure that the statement adheres to our policy

Data are available at http://doi.org/10.6084/m9.figshare.23302427

Research involving human participants, their data, or biological material

	studies with <u>human participants or human data</u> . See also policy information about <u>sex, gender (identity/presentation)</u> , and <u>race, ethnicity and racism</u> .	
Reporting on sex ar	ender N/A	
Reporting on race, other socially relev groupings	nicity, or N/A	
Population charact	tics N/A	
Recruitment	N/A	
Ethics oversight	Identify the organization(s) that approved the study protocol.	
Note that full information	n the approval of the study protocol must also be provided in the manuscript.	
- ield-spec	ic reporting	
Please select the one	ow that is the best fit for your research. If you are not sure, read the appropriate sections before making your selection.	
X Life sciences	Behavioural & social sciences Ecological, evolutionary & environmental sciences	
For a reference copy of the	ument with all sections, see <u>nature.com/documents/nr-reporting-summary-flat.pdf</u>	
_ife sciend	s study design	
All studies must discl	on these points even when the disclosure is negative.	
r f t c H	ble sizes were chosen based on our previous experiments of 1) the intra- and inter-donor culture variability of ASL height data, and 2) ents which stimulate chloride secretion (CFTR and CaCC). Bessay is well established for measuring water flux from airway epithelial cultures and is used as an FDA endpoint for chloride-mediated eff Vertex Pharmaceuticals). We have a long published history of using this technique and use sample sizes based on our analysis of the nical/experimental error and donor-to-donor variability. The donor and replicate size for this study was selected to statistically rentiate a change in ASL volume of 0.5 μm between groups. Bare some historical references for this approach: Barsui H, et. al. Evidence for periciliary liquid layer depletion, not abnormal ion composition, in the pathogenesis of cystic fibrosis airways see. Cell. 1998 Dec 23;95(7):1005–15. PMID: 9875854 Barsun R, et. al. The relative roles of passive surface forces and active ion transport in the modulation of airway surface liquid volume and position. J Gen Physiol. 2001;118(2):223–236. PMID: 11479349	e 'S
Data exclusions	usions were made.	
	Studies were performed replicate cultures from primary cells from three different donor lungs (all non-diseased) Randomization. All studies in different donors and replicate cultures performed here were consistent with our presented findings.	
Randomization Analysis of control vs. test agent was performed in replicate cultures from the same donor. Here, random cultures were assigned to be control or the actual test.		er

Reporting for specific materials, systems and methods

test agents were performed by a different person than the one doing the subsequent analysis.

Blinding

We require information from authors about some types of materials, experimental systems and methods used in many studies. Here, indicate whether each material, system or method listed is relevant to your study. If you are not sure if a list item applies to your research, read the appropriate section before selecting a response.

Only ASL height studies require Blinding. Treatment of cultures used for ASL height studies blinded. Here, treatment of cultures with control &

۵	b	
τ		
i	2	
	-	
2		
ŗ		

Materials & experimental s	ystems Methods
n/a Involved in the study	n/a Involved in the study
Antibodies	ChIP-seq
☐ Eukaryotic cell lines	Flow cytometry
Palaeontology and archaeo	ogy MRI-based neuroimaging
Animals and other organism	IS IS
Clinical data	
Dual use research of concer	n
Eukaryotic cell lines Policy information about cell lines	and Sex and Gender in Research
Cell line source(s)	Primary human airway cells from CF donor lungs
Authentication	Cells were obtained directly from the lungs by our group using well established protocols (referenced in manuscript). Prior to the study, histological studies were performed to ensure the correct pheontype of CF airway epithelial cells (i.e., fluid hyperabsorbing was observed.
Mycoplasma contamination	Only primary cell lines are used (i.e., not immortalized cell lines) and our cultures are used for only 30-45 days prior to disposal. However, our incubators are checked for mycoplasma contamination if aberrant results are obtained with our cells or on notification of a positive result with our cell isolation group.
Commonly misidentified lines	N/A

(See <u>ICLAC</u> register)